Accurate simulation of frictionless and frictional cohesive crack growth in quasi-brittle materials using XFEM

B.L. Karihaloo & Q.Z. Xiao
School of Engineering, Cardiff University, Queen's Buildings, The Parade, Newport Road, Cardiff CF24 3AA, UK

ABSTRACT: This paper discusses the crack tip asymptotic fields of frictionless and frictional cohesive cracks in quasi-brittle materials. This has been made possible after reformatting the cohesive-law into a special but universal polynomial. For accurate simulation of crack growth in quasi-brittle materials using the extended/generalized finite element method (XFEM), the leading term of the true displacement asymptotic field is used as the enrichment function at the tip of a cohesive crack. The opening component of the same field is also used as the initial guess opening profile of a newly extended cohesive segment. A statically admissible stress recovery (SAR) technique is used to recover the stresses at the crack tip. Finally, a pure mode I cohesive crack problem is analysed to demonstrate the characteristics of global responses and local fields obtained numerically by the XFEM.

1 INTRODUCTION

The cohesive zone (or crack) model of Hillerborg et al. (1976) has been extensively used in the study of localisation and failure in quasi-brittle materials and structures. Elices et al. (2002) have discussed its advantages and limitations. In the most widely used standard formulation of the model (see Fig. 1 below), it is assumed that the stress–strain behaviour is isotropic linear elastic, and that the crack is initiated at a point where the maximum tensile principal stress σ_1 reaches the tensile strength f_t of the uncracked material, and that the crack is oriented normal to the direction of σ_1. An evolution law is also postulated for the monotonic mode I loading so that the cohesive stress is a unique function of the crack opening which, for concrete, decreases monotonically along the cohesive zone. The cohesive crack propagates when σ_1 at its tip reaches f_t. Although this standard formulation of the cohesive crack model is highly simplified, it is able to capture the essence of the fracture process in concrete specimens and structures (see Karihaloo 1995).

de Borst et al. (2004) have given a concise overview of the various ways to numerically implement the cohesive zone methodology. They concluded that the extended/generalized finite element method (XFEM) (Moës et al. 1999, Strouboulis et al. 2001, Karihaloo & Xiao 2003b, Xiao & Karihaloo 2005) provides a proper representation of the discrete character of cohesive zone formulations avoiding any mesh bias. The XFEM enriches the standard local FE approximations with known information about the problem, such as a displacement discontinuity across a crack, the asymptotic solution at a crack tip, or a strain discontinuity across an interface, with the use of the partition of unity (PU). In contrast with the FEM, it avoids the use of meshes conforming with the discontinuity and adaptive remeshing as the discontinuity grows.

In the XFEM formulation of the cohesive zone model, Wells and Sluys (2001) used the jump function as an enrichment function for the whole cohesive crack, hence the cohesive crack tip touches the element boundary. Moës and Belytschko (2002) used the jump function for the part of the cohesive crack not adjacent to its tip, and a branch function adjacent to the tip. This approach can handle cases in which the cohesive crack tip does not touch the element boundary. However, the adopted branch

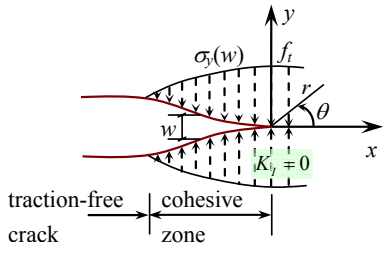

Figure 1. A real traction-free crack terminating in a fracture process (cohesive) zone (FPZ) with residual stress transfer capacity $\sigma_y(w)$ whose faces close smoothly near its tip ($K_I = 0$). The material outside the FPZ is linear elastic, but within the FPZ is softening.

function does not represent the true asymptotic nature of the displacement/stress field adjacent to the cohesive crack tip. Hansbo and Hansbo (2004) modelled strong and weak discontinuities in solid mechanics by considering an element traversed by a discontinuity as a double element each half of which is used for the interpolation of one side of the discontinuity. This approach is difficult to use when the discontinuity ends within an element. Zi and Belytschko (2003) enriched all cracked linear3-node or quadratic 6-node triangular elements including the elements containing the crack tip by the sign function. Alfaiate et al. (2003) embedded displacement jumps which do not need to be homogeneous within each FE. Mariani and Perego (2003) introduced in a standard FE model a cubic displacement discontinuity, in order to reproduce the typical cusp-like shape of the process zone at the tip of a cohesive crack. However, this cubic function does not represent the true angular distribution of the displacement adjacent to the tip.

The lack of any work on the asymptotic fields at the tip of a cohesive crack is surprising considering the widespread use of cohesive crack models. This blank has been recently filled by Xiao and Karihaloo (2006b) who obtained universal asymptotic expansions at a cohesive crack tip, analogous to Williams expansions at a traction-free crack tip. Coulomb friction on the cohesive crack faces is also considered. The coefficients of the expansions of course depend nonlinearly on the softening-law and the boundary conditions. These universal expansions are valid for any normal cohesion-separation law (i.e. softening law) that can be expressed in a special polynomial form. They demonstrated that many commonly-used cohesion-separation laws, e.g. rectangular, linear, bilinear and exponential, can be expressed in this special form.

In this paper, we will summarize the reformulated polynomial softening-law and the crack tip asymptotic fields of frictionless and frictional cohesive cracks in quasi-brittle materials given by Xiao and Karihaloo (2006b). We will use the leading term of the true displacement asymptotic field at the tip of a cohesive crack as the enrichment function in the XFEM. The opening component of the same field is also used as the initial guess opening profile of a newly extended cohesive segment. The tip of the growing cohesive crack does not have to terminate on an element boundary.

Rubinstein (2003) has shown that relatively small errors in the determination of the crack path deflection angle can lead to a significant cumulative deviation of the crack path over a finite crack length. Therefore a reliable analysis of cohesive crack propagation requires an accurate knowledge of the crack tip field. In order to obtain accurate angular distribution of the stress adjacent to the crack tip, a statically admissible stress recovery (SAR) scheme (Xiao & Karihaloo 2004, 2006a, Xiao et al. 2007) will be adopted. SAR uses basis functions, which meet the equilibrium equations within the domain and the local traction conditions on the boundary, and moving least squares (MLS) to fit the stresses at sampling (e.g., quadrature) points obtained by the XFEM. The most widely used stress recovery scheme (denoted as AVG) will also be used for comparison. AVG simply averages the stress values at each node evaluated from adjacent elements by bi-linear extrapolation from the Gauss points, and interpolates the averaged stresses using shape functions.

We will analyse a notched flexural specimen made of quasi-brittle materials with a bilinear law and show that the growth of a cohesive crack in a quasi-brittle material can be accurately predicted with a very coarse mesh which is not possible with the FEM. We will also demonstrate the characteristics of global responses and local fields obtained numerically by the XFEM.

2 POLYNOMIAL COHESIVE LAW FOR QUASI-BRITTLE MATERIALS

In order to obtain the separable asymptotic field at a cohesive crack tip (in terms of r and θ functions, r and θ are local polar coordinates centered at the tip, see Fig. 1) in quasi-brittle materials like concrete, Xiao and Karihaloo (2006b) reformulated the softening law into the following polynomial

$$\frac{\sigma}{f_t}=1+\sum_{i=1}^{5}\alpha_i\left(\frac{w}{w_c}\right)^{\frac{2}{3}i}-\left(1+\sum_{i=1}^{5}\alpha_i\right)\left(\frac{w}{w_c}\right)^4 \tag{1}$$

or in normalized form

$$\hat{\sigma}_y=1+\sum_{i=1}^{5}\alpha_i\hat{w}^{\frac{2}{3}i}-\left(1+\sum_{i=1}^{5}\alpha_i\right)\hat{w}^4 \tag{2}$$

where σ and f_t are the stress normal to the cohesive crack face and the uniaxial tensile strength, respectively; w and w_c are the opening displacement of the cohesive crack faces, and the critical opening displacement of the pre-existing macrocrack tip when it begins to grow; α_i, $i = 1 \sim 5$, are fitting parameters. Relation (1) or (2) can represent a wide variety of softening laws.

For example, the widely used linear softening law

$$\frac{\sigma}{f_t}=1-\frac{w}{w_c} \tag{3}$$

can be represented by (1) with the only non-vanishing coefficients α_1 = -0.2612, α_2 = -1.0215, i.e.

$$\hat{\sigma}_y=1+\alpha_1\hat{w}^{\frac{2}{3}}+\alpha_2\hat{w}^{\frac{4}{3}}-(1+\alpha_1+\alpha_2)\hat{w}^2 \tag{4}$$

The correlation coefficient is 1. The linear law (3) is compared with (1) or (4) in Fig. 2; they cannot be distinguished on the scale of the figure.

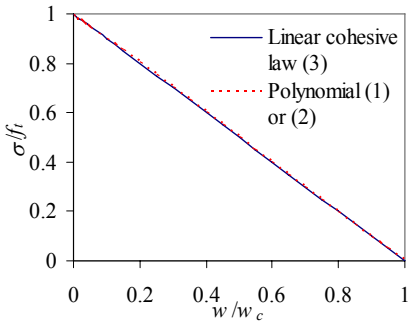

Figure 2. Linear tension-softening law.

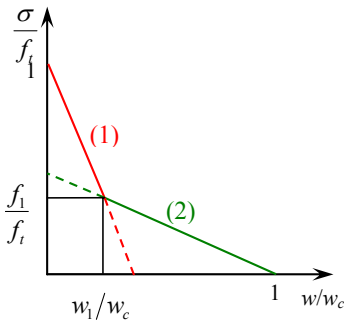

Figure 3. Bilinear tension-softening law.

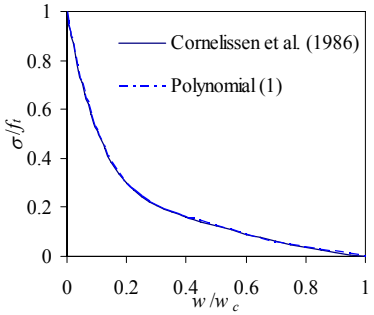

Figure 4. Cohesive law (8).

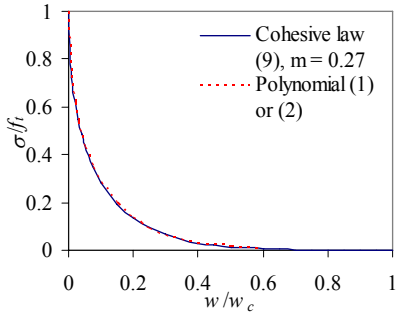

Figure 5. Cohesive law (9).

Similarly, for the widely used bilinear tension-softening law (Fig. 3)

$$\hat{\sigma}=\begin{cases}1-\left(1-\hat{f}_1\right)\dfrac{\hat{w}}{\hat{w}_1}, & 0\le\hat{\sigma}\le\hat{f}_1\\ \dfrac{\hat{f}_1}{1-\hat{w}_1}\left(1-\hat{w}\right), & \hat{f}_1<\hat{\sigma}\le 1\end{cases} \tag{5}$$

($\hat{f}_1=f_1/f_t$, $\hat{w}_1=w_1/w_c$), its two linear parts can be rewritten into two linear laws as shown in Fig. 3. The first part can be written into (4) using a new definition of w_c as

$$w_c=\frac{w_1}{1-\hat{f}_1} \tag{6}$$

The second part can be written into (4) using a new definition of f_t as

$$f_t=\frac{f_1}{1-\hat{w}_1} \tag{7}$$

Cornelissen et al. (1986) introduced the following exponential relation

$$\frac{\sigma}{f_t}=f\left(\frac{w}{w_c}\right)-\frac{w}{w_c}f(1),\quad f\left(\frac{w}{w_c}\right)=\left[1+\left(C_1\frac{w}{w_c}\right)^3\right]e^{-C_2\frac{w}{w_c}} \tag{8}$$

C_1 and C_2 are fitting parameters. For a normal concrete (NC) with density 2370 kg/m^3, compressive strength f_c = 47 MPa, Young modulus E = 39 GPa, f_t = 3.2 MPa, w_c = 160 μm, specific fracture energy G_F = 100 J/m^2 (area under the tension-softening curve), C_1 = 3 and C_2 = 6.93. This diagram can also be fitted by (1) with α_1 = -0.872, α_2 = -16.729, α_3 = 67.818, α_4 = -110.462, and α_5 = 83.158. The correlation coefficient is 1. They are compared in Fig. 4, and cannot be distinguished on the scale of the figure.

Wecharatana (1990) introduced the following softening relationship

$$\hat{\sigma}^m+\hat{w}^{2m}=1 \tag{9}$$

m = 0.27 for concrete with compressive strength f_c = 24 MPa. In the range of $0\le\hat{w}\le 0.6$, we can fit (9) using (1) with α_1 = -6.9495, α_2 = 29.9794, α_3 = -87.2663, α_4 = 148.3647, and α_5 = -128.84. The correlation coefficient is 1. When $\hat{w}$ = 0.6, $\hat{\sigma}$ = 0.005148; when $\hat{w}$ > 0.6, $\hat{\sigma}$ is negligibly small. As compared in Fig. 5, they cannot be distinguished on the scale of the figure.

3 CRACK TIP ASYMPTOTIC FIELDS OF FRICTIONLESS AND FRICTIONAL COHESIVE CRACKS IN QUASI-BRITTLE MATERIALS

Muskhelishvili (1953) showed that, for plane problems, the stresses and displacements in the Cartesian coordinate system (see Fig. 1) can be expressed in terms of two analytic functions $\phi(z)$ and $\chi(z)$ of the complex variable $z = re^{i\theta}$

$$\begin{aligned}&\sigma_x+\sigma_y=2[\phi'(z)+\overline{\phi'(z)}]\\&\sigma_y-\sigma_x+2i\tau_{xy}=2[\bar{z}\phi''(z)+\chi''(z)]\\&2\mu(u+iv)=\kappa\phi(z)-z\overline{\phi'(z)}-\overline{\chi'(z)}\end{aligned} \tag{10}$$

where a prime denotes differentiation with respect to z and an overbar complex conjugate. In (10), $\mu=E/[2(1+\nu)]$ is the shear modulus; the Kolosov constant is $\kappa=3-4\nu$ for plane strain or $\kappa=(3-\nu)/(1+\nu)$ for plane stress.

For a general plane mixed mode I + II problem, the complex functions $\phi(z)$ and $\chi(z)$ can be chosen as series of complex eigenvalue Goursat functions (Sih & Liebowitz 1968, Karihaloo & Xiao 2003a)

$$\phi(z)=\sum_{n=0}A_nz^{\lambda_n}=\sum_{n=0}A_nr^{\lambda_n}e^{i\lambda_n\theta}\qquad\chi(z)=\sum_{n=0}B_nz^{\lambda_n+1}=\sum_{n=0}B_nr^{\lambda_n+1}e^{i(\lambda_n+1)\theta} \tag{11}$$

where the complex coefficients are $A_n = a_{1n} + ia_{2n}$ and $B_n = b_{1n} + ib_{2n}$. The eigenvalues λ_n and coefficients a_{1n}, a_{2n}, b_{1n} and b_{2n} are real.

The asymptotic analysis of the crack tip fields needs to satisfy the proper symmetry conditions along the line of extension of the cohesive crack, and boundary conditions on the cohesive crack faces.

If normal cohesive separation applies to the crack faces, relationship (1) needs to be satisfied over the cohesive zone. The stresses at the cohesive crack tip are non-singular (because the stress intensity factor $K_I = 0$). Moreover, the following conditions need to be satisfied:

(a) if the Coulomb friction on the crack face is considered

$$\sigma_y\big|_{\theta=\pi} = \sigma_y\big|_{\theta=-\pi} \neq 0, \tau_{xy}\big|_{\theta=\pi} = \tau_{xy}\big|_{\theta=-\pi} = -\mu_f \sigma_y\big|_{\theta=\pm\pi} \neq 0 \tag{12}$$

where μ_f equals the positive or negative value of the coefficient of kinetic friction, which is assumed to be constant, depending on the relative sliding direction of the two crack faces: $\mu_f > 0$ when relative sliding $\delta > 0$ and $\mu_f < 0$ when $\delta < 0$. When $\mu_f = 0$, the cohesive crack faces are frictionless.

(b) if the cohesive crack faces are in pure mode I condition

$$\sigma_y\big|_{\theta=\pi} = \sigma_y\big|_{\theta=-\pi} \neq 0, \tau_{xy}\big|_{\theta=\pi} = \tau_{xy}\big|_{\theta=-\pi} = 0, \tau_{xy}\big|_{\theta=0} = 0 \text{ and } v\big|_{\theta=0} = 0 \tag{13}$$

The length of the process (cohesive) zone is determined by the condition $w \le w_c$ in the normally opened part of the crack.

For a Coulomb frictional cohesive crack with normal cohesive separation (1), the complete asymptotic solutions are composed of two parts. The first part corresponds to integer eigenvalues

$$\lambda_n = n + 1, \quad b_{2n} = -\frac{n}{n+2} a_{2n} - \mu_f (a_{1n} + b_{1n}), \; n = 0, 1, 2, \ldots \tag{14}$$

$$\sigma_y\big|_{\theta=\pm\pi} = \sum_{n=0} (n+2)(n+1) r^n (a_{1n} + b_{1n}) \cos n\pi$$

$$\text{or} \quad \hat{\sigma}_y = \frac{\sigma_y\big|_{\theta=\pm\pi}}{f_t} = \sum_{n=0} c_n r^n = 1 + \sum_{n=1} c_n r^n \tag{15}$$

where

$$c_n = \frac{(n+2)(n+1)(a_{1n} + b_{1n}) \cos n\pi}{f_t}, \; c_0 = \frac{2(a_{10} + b_{10})}{f_t} = 1 \tag{16}$$

since $\sigma_y\big|_{\theta=\pm\pi} = f_t$ when $r \to 0$. These solutions have non-zero σ_y and τ_{xy} along the cohesive crack faces, but zero crack opening w and sliding δ. The second part of the asymptotic solutions corresponds to non-integer eigenvalues

$$\lambda_n = \frac{2n+3}{2}, \quad b_{1n} = -\frac{2n+1}{2n+5} a_{1n}, \quad b_{2n} = -a_{2n}, \; n = 0, 1, 2, \ldots \tag{17}$$

$$w = \sum_{n=0} \frac{r^{\frac{2n+3}{2}}}{\mu} \left[\left(\kappa + \frac{2n+3}{2} \right) a_{1n} + \frac{2n+5}{2} b_{1n} \right] \sin \frac{2n+3}{2} \pi$$

or

$$\hat{w} = \frac{w}{w_c} = \sum_{n=0} \bar{d}_n r^{\frac{2n+3}{2}} \quad \bar{d}_n = \frac{\left[\left(\kappa + \frac{2n+3}{2} \right) a_{1n} + \frac{2n+5}{2} b_{1n} \right] \sin \frac{2n+3}{2} \pi}{\mu w_c} \tag{18}$$

Consider the truncated $N + 1$ terms of $\hat{w}$ (18), and denote $d_0 = \bar{d}_0$, $d_n = \bar{d}_n / d_0$ $(n > 1)$

$$\hat{w} = d_0 r^{\frac{3}{2}} \left(1 + \sum_{n=1}^{N} d_n r^n \right) \tag{19}$$

The expansion of $\hat{w}$ (19) raised to the power $2i/3$ is also truncated to $N + 1$ terms, since these terms include only the truncated $N + 1$ terms of $\hat{w}$. Hence

$$\hat{w}^{\frac{2i}{3}} = d_0^{\frac{2i}{3}} r^i \left(1 + \sum_{n=1}^{N} \beta_{in} r^n \right) \tag{20}$$

where

$$\beta_{in} = \frac{f_i^{(n)}(0)}{n!}, \quad f_i(r) = \left(1 + \sum_{n=1}^{N} d_n r^n \right)^{\frac{2i}{3}} \tag{21}$$

and $f_i^{(n)}(0)$ denotes the nth derivative at $r = 0$. The first five coefficients β_{in} are

$$\beta_{i1} = \frac{2}{3} i d_1$$

$$\beta_{i2} = \frac{1}{3} i \left(\frac{2}{3} i - 1 \right) d_1^2 + \frac{2}{3} i d_2$$

$$\beta_{i3} = \frac{1}{9} i \left(\frac{2}{3} i - 1 \right) \left(\frac{2}{3} i - 2 \right) d_1^3 + \frac{2}{3} i \left(\frac{2}{3} i - 1 \right) d_1 d_2 + \frac{2}{3} i d_3$$

$$\begin{aligned} \beta_{i4} = {} & \frac{1}{36} i \left(\frac{2}{3} i - 1 \right) \left(\frac{2}{3} i - 2 \right) \left(\frac{2}{3} i - 3 \right) d_1^4 + \frac{1}{3} i \left(\frac{2}{3} i - 1 \right) \left(\frac{2}{3} i - 2 \right) d_1^2 d_2 \\ & + \frac{1}{3} i \left(\frac{2}{3} i - 1 \right) d_2^2 + \frac{2}{3} i \left(\frac{2}{3} i - 1 \right) d_1 d_3 + \frac{2}{3} i d_4 \end{aligned} \tag{22}$$

$$\begin{aligned} \beta_{i5} = {} & \frac{1}{180} i \left(\frac{2}{3} i - 1 \right) \left(\frac{2}{3} i - 2 \right) \left(\frac{2}{3} i - 3 \right) \left(\frac{2}{3} i - 4 \right) d_1^5 \\ & + \frac{1}{9} i \left(\frac{2}{3} i - 1 \right) \left(\frac{2}{3} i - 2 \right) \left(\frac{2}{3} i - 3 \right) d_1^3 d_2 \\ & + \frac{1}{3} i \left(\frac{2}{3} i - 1 \right) \left(\frac{2}{3} i - 2 \right) d_1 d_2^2 + \frac{1}{3} i \left(\frac{2}{3} i - 1 \right) \left(\frac{2}{3} i - 2 \right) d_1^2 d_3 \\ & + \frac{2}{3} i \left(\frac{2}{3} i - 1 \right) d_2 d_3 + \frac{2}{3} i \left(\frac{2}{3} i - 1 \right) d_1 d_4 + \frac{2}{3} i d_5 \end{aligned}$$

If we choose $N = 5$, then after satisfying the cohesive relationship (1) we have the following expressions for coefficients c_n in (16)

$$c_1 = \alpha_1 d_0^{\frac{2}{3}}$$

$$c_2 = \alpha_2 d_0^{\frac{4}{3}} + \alpha_1 d_0^{\frac{2}{3}} \beta_{11}$$

$$c_3 = \alpha_3 d_0^2 + \alpha_1 d_0^{\frac{2}{3}} \beta_{12} + \alpha_2 d_0^{\frac{4}{3}} \beta_{21}$$

$$c_4 = \alpha_4 d_0^{\frac{8}{3}} + \alpha_1 d_0^{\frac{2}{3}} \beta_{13} + \alpha_2 d_0^{\frac{4}{3}} \beta_{22} + \alpha_3 d_0^2 \beta_{31}$$

$$c_5 = \alpha_5 d_0^{\frac{10}{3}} + \alpha_1 d_0^{\frac{2}{3}} \beta_{14} + \alpha_2 d_0^{\frac{4}{3}} \beta_{23} + \alpha_3 d_0^2 \beta_{32} + \alpha_4 d_0^{\frac{8}{3}} \beta_{41}$$

$$c_6 = \alpha_1 d_0^{\frac{2}{3}}\beta_{15} + \alpha_2 d_0^{\frac{4}{3}}\beta_{24} + \alpha_3 d_0^{2}\beta_{33} + \alpha_4 d_0^{\frac{8}{3}}\beta_{42} + \alpha_5 d_0^{\frac{10}{3}}\beta_{51} - \left(1+\sum_{i=1}^{5}\alpha_i\right) d_0^4$$

$$c_7 = \alpha_2 d_0^{\frac{4}{3}}\beta_{25} + \alpha_3 d_0^{2}\beta_{34} + \alpha_4 d_0^{\frac{8}{3}}\beta_{43} + \alpha_5 d_0^{\frac{10}{3}}\beta_{52} - \left(1+\sum_{i=1}^{5}\alpha_i\right) d_0^4\beta_{61}$$

$$c_8 = \alpha_3 d_0^{2}\beta_{35} + \alpha_4 d_0^{\frac{8}{3}}\beta_{44} + \alpha_5 d_0^{\frac{10}{3}}\beta_{53} - \left(1+\sum_{i=1}^{5}\alpha_i\right) d_0^4\beta_{62}$$

$$c_9 = \alpha_4 d_0^{\frac{8}{3}}\beta_{45} + \alpha_5 d_0^{\frac{10}{3}}\beta_{54} - \left(1+\sum_{i=1}^{5}\alpha_i\right) d_0^4\beta_{63}$$

$$c_{10} = \alpha_5 d_0^{\frac{10}{3}}\beta_{55} - \left(1+\sum_{i=1}^{5}\alpha_i\right) d_0^4\beta_{64}$$

$$c_{11} = -\left(1+\sum_{i=1}^{5}\alpha_i\right) d_0^4\beta_{65} \tag{23}$$

For non-integer eigenvalues (17), the coefficients a_{1n} and a_{2n} may be regarded as independent, so that coefficients b_{1n} are linearly dependent on a_{1n} and b_{2n} on a_{2n}. For integer eigenvalues (14), coefficients a_{1n} and a_{2n} may also be regarded as independent, so that coefficients b_{2n} now depend linearly on a_{1n}, a_{2n} and b_{1n}. However, the coefficients b_{1n} for integer eigenvalues will depend both linearly on a_{1n} for integer eigenvalues and nonlinearly on a_{1n} for non-integer eigenvalues via (16), (18), (19), (21) and (23). The inherent nonlinear nature of the problem is reflected in these nonlinear relationships between the coefficients of the asymptotic fields.

Note that the above asymptotic solution cannot be reduced to a pure mode I cohesive crack (compare (12) and (13)), since along the line of extension of the crack, $\theta = 0$, the shear stress does not vanish ($\tau_{xy} \neq 0$). However, the procedures are similar; and the complete asymptotic fields have been given by Xiao and Karihaloo (2006b). The first term corresponding to a non-integer eigenvalue that gives a normal displacement discontinuity over the cohesive crack faces is

$$u = \frac{r^{3/2}}{2\mu} a_1 \left[\left(\kappa+\frac{1}{2}\right)\cos\frac{3}{2}\theta - \frac{3}{2}\cos\frac{1}{2}\theta\right]$$
$$v = \frac{r^{3/2}}{2\mu} a_1 \left[\left(\kappa-\frac{1}{2}\right)\sin\frac{3}{2}\theta - \frac{3}{2}\sin\frac{1}{2}\theta\right] \tag{24}$$

4 SIMULATION OF COHESIVE CRACK GROWTH IN QUASI-BRITTLE MATERIALS USING XFEM

To model the cohesive cracks in the XFEM, a standard local FE displacement approximation around the crack is enriched with discontinuous Heaviside functions along the crack faces behind the crack tip including the open traction-free part, and the crack tip asymptotic displacement fields at nodes surrounding the cohesive crack tip using the PU. The approximation of displacements for an element can be expressed in the following form

$$\begin{Bmatrix} u^h(x) \\ v^h(x) \end{Bmatrix} = \sum_{i\in I} \phi_i(x) \begin{Bmatrix} u_{0i} \\ v_{0i} \end{Bmatrix} + \sum_{j\in J\cap I} \phi_j(x) H(x) \begin{Bmatrix} b_{1j} \\ b_{2j} \end{Bmatrix} + \sum_{m\in M_k\cap I} \phi_m(x) \begin{Bmatrix} u_m^{(tip\,k)} \\ v_m^{(tip\,k)} \end{Bmatrix} \tag{25}$$

where I is the set of all nodes in the element, (u_{0i}, v_{0i}) are the regular degrees of freedom at node i, ϕ_i is the FE shape function associated with node i, J is the subset of nodes whose support is intersected by the crack but do not cover any cohesive crack tips, the function $H(x)$ is the Heaviside function centred on the crack discontinuity, and (b_{1j}, b_{2j}) are the corresponding additional degrees of freedom. M_k is the subset of nodes that are enriched around the cohesive crack tip k with the asymptotic displacements $u^{(\text{tip } k)}$ and $v^{(\text{tip } k)}$. $u_m^{(tip\,k)}$ and $v_m^{(tip\,k)}$ are enrichment functions adopted at node m with corresponding nodal parameters independent of other nodes.

Consider a domain Ω containing a crack Γ_c, as shown in Fig. 6. The boundary Γ is composed of the segments Γ_u, Γ_t, and Γ_c. The part of the crack on which a softening law is active, i.e. the FPZ, is denoted by Γ_{coh}. Prescribed displacements $\bar{\boldsymbol{u}}$ are imposed on Γ_u, while tractions $\boldsymbol{F}$ are imposed on Γ_t. The crack surface Γ_c excluding Γ_{coh} is assumed to be traction-free. The cohesive tractions $\boldsymbol{t}^+$, $\boldsymbol{t}^-$ are imposed on the upper and lower surfaces of Γ_{coh}.

The virtual work equation without body forces is given by Wells and Sluys (2001) and Moës and Belytschko (2002)

$$\int_\Omega \boldsymbol{\sigma}(\boldsymbol{u}) : \nabla^s \boldsymbol{v} d\Omega + \int_{\Gamma_{coh}} \boldsymbol{t}\cdot\boldsymbol{w}(\boldsymbol{v}) d\Gamma = \int_{\Gamma_t} \boldsymbol{F}\cdot\boldsymbol{v} d\Gamma \tag{26}$$

where $\boldsymbol{\sigma}$ is the Cauchy stress, and ∇^s denotes the symmetric part of the gradient operator. The displacements $\boldsymbol{u}$ must belong to the space U of kinematically admissible displacement fields

$$\boldsymbol{u} \in U = \left\{\boldsymbol{u} \in U : \boldsymbol{u} = \bar{\boldsymbol{u}} \text{ on } \Gamma_u, \boldsymbol{u} \text{ discontinuous on } \Gamma_c\right\} \tag{27}$$

where the space U is related to the regularity of the solution. The test function $\boldsymbol{v}$ must belong to the

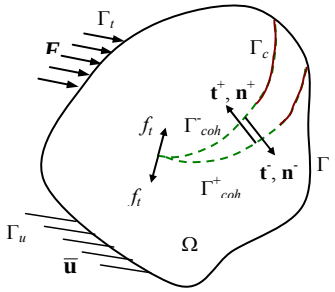

Figure 6. Body with a crack Γ_c involving a cohesive zone Γ_{coh} subjected to prescribed boundary tractions $\boldsymbol{F}$ on Γ_t and displacements $\bar{\mathbf{u}}$ on Γ_u.

space V defined by

$$\boldsymbol{v} \in V = \{\boldsymbol{v} \in V : \boldsymbol{v} = 0 \text{ on } \Gamma_u, \boldsymbol{v} \text{ discontinuous on } \Gamma_c\} \tag{28}$$

The cohesive tractions $\boldsymbol{t} = \boldsymbol{t}^+ = -\boldsymbol{t}^-$ and the separation $\boldsymbol{w}(\boldsymbol{v}) = \boldsymbol{v}^- - \boldsymbol{v}^+$ are related by a softening law on Γ_{coh}.

For a softening law composed of linear segments, equation (26) can be solved using a secant modulus iteration scheme when the length of the cohesive zone and external loads are given. The term secant modulus here refers to the fact that the stiffness matrix of XFEM obtained from (26) relates directly the total displacements to loads. Displacements (24) are used as the crack tip enrichment function in (25) for a mode I cohesive crack. The unknown coefficient a_1 depends on the softening law, and boundary and load conditions. It is considered as additional degrees of freedom at relevant enrichment nodes in XFEM. Details of the implementation of XFEM, SAR, and simulation of cohesive crack growth can be found in Xiao et al. (2007).

5 ILLUSTRATION OF THE MODE I COHESIVE CRACK TIP FIELDS

In order to visualise the cohesive crack tip fields derived in Section 3, it is necessary to determine the unknown coefficients by fitting the numerically computed crack tip fields with the theoretically obtained fields. This requires a sophisticated optimization scheme. For the present purpose of illustration, we will solve a mode I cohesive crack problem shown in Fig. 7 using the obtained asymptotic fields and the numerically computed opening profile of the cohesive crack.

We consider the subdomain bounded by broken lines in Fig. 7, and assume the length of the cohesive crack is 10.5 mm. The opening profile of the cohesive crack (Fig. 8) adopts the computed results of a three point bend beam with a very small initial crack of length 0.1mm at the bottom midpoint of the beam (Fig. 9) at the loading stage with total cohesive crack = 31.5mm and load/($f_t bt$) = 0.228 (Xiao & Karihaloo 2006b). The geometrical parameters are b = 150 mm, $l = 4b$, $t = b$ (t is the specimen thickness in the out-of-plane direction). A linear softening law and a state of plane strain condition are considered. The material properties are E = 36.5 GPa, ν = 0.1, f_t = 3.19MPa, G_F = 50 N/m. The dimensions for force and length are N and mm, respectively.

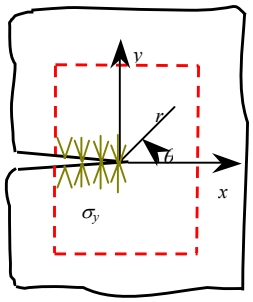

Figure 7. Illustration of the cohesive crack problem.

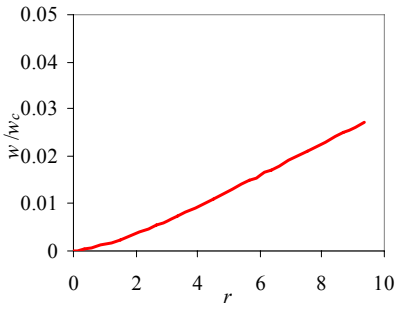

Figure 8. Opening profile of the cohesive crack.

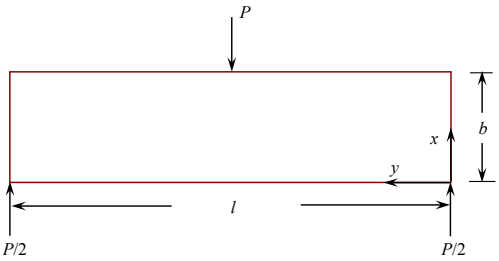

Figure 9. A three-point bend beam (TPB).

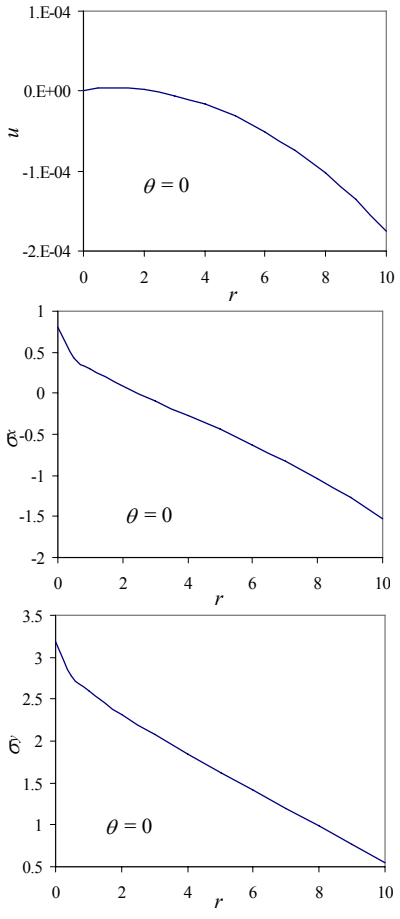

Figure 10. Non-vanishing displacements and stresses along the line of extension of the cohesive crack ($\theta = 0$).

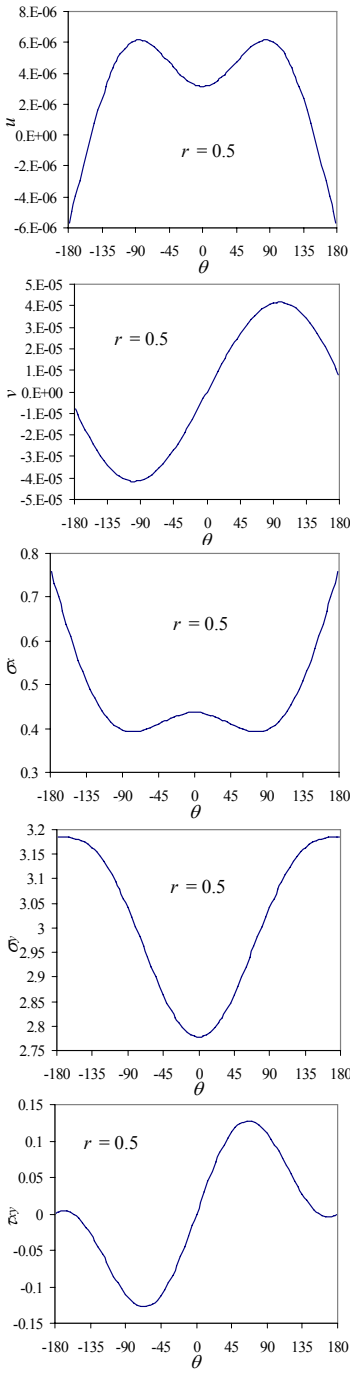

Figure 11. Displacements and stresses along the circle $r = 0.5$.

The displacements and stresses along the line of extension of the cohesive crack and the circle with radius $r = 0.5$ mm surrounding the crack tip are plotted in Figs. 10 and 11. As expected, the stress σ_y at the cohesive crack tip is equal to f_t, and no stress at any other locations reaches f_t.

6 NUMERICAL EXAMPLE

In this section, we will analyse an edge cracked plate under uniaxial tension (Fig. 12). The geometrical parameters are $b = 150$ mm, $l = 4b$, $t = b$. A state of plane strain condition is considered. The initial edge crack has a length of $a_0 = 15.1$mm. The properties $E = 36.9$ GPa, $\nu = 0.2$, and a bilinear softening law (5) with $f_t = 3.14$ MPa, $f_1 = 0.455$ MPa, $w_c = 0.279$ mm, $w_1 = 0.0373$ mm, $G_F = 122$ N/m, obtained by Abdalla and Karihaloo (2004) for a real normal strength concrete are used.

Two meshes, as shown in Fig. 13, are used in the analysis. The coarser mesh consists of 50×100 = 5000 rectangular elements, giving a total of 5151 nodes. The finer mesh consists of 150×120 = 18000 rectangular elements, giving a total of 18271 nodes. Both meshes are uniformly divided in x-direction. For the coarser mesh, the central 50 layers of elements have an identical height (y-direction) of 3mm; the remaining elements have an identical height of 9mm. Therefore, elements in the central zone are 3×3 mm^2 squares. For the finer mesh, the central 60 layers of elements have an identical height of 1mm; the remaining elements have an identical height of 9mm. Therefore elements in the central zone are 1×1 mm^2 squares. We will study global responses including the load – deformation behaviour and the evolution of the cohesive zone, as well as local properties including the opening profile and distribution of the cohesive stress in the cohesive zone, and displacements and stresses along the circle $r = 3.5$mm (the second layer of elements in the coarser mesh, or the fourth layer of elements in the finer mesh) around the crack tip and along the line of extension of the crack. The intention of using two meshes is to study the mesh size sensitivity of the global responses as well as of the crack tip fields. Furthermore, the results from the finer mesh will be used as a reference solution, since no analytical solutions are available. The conventional 4-node bilinear isoparametric Q4 elements are used as background elements. The potential fracture locus coincides with the specimen's axis of symmetry. The crack is modelled by enriching the nodes on the crack faces with jump without the double nodes that are used in the traditional FEM.

The first layer of nodes surrounding the cohesive crack tip are enriched with (24). The opening component of the same field is also used as the initial opening profile of a newly extended cohesive segment in the simulation of cohesive crack propagation.

Similar to Moës and Belytschko (2002), x-direction of nodes with coordinates (0, 0) and (0, 600mm) and y-direction of the node with coordinates (150mm, 300mm) are constrained; the load is distributed over a length of 6mm for the coarse mesh and 2mm for the fine mesh (two elements).

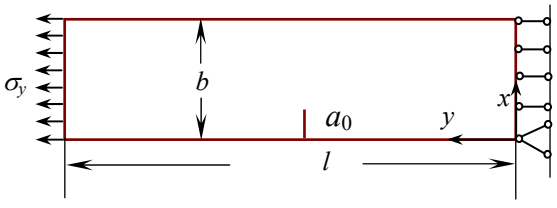

Figure 12. An edge-cracked plate under uniaxial tension.

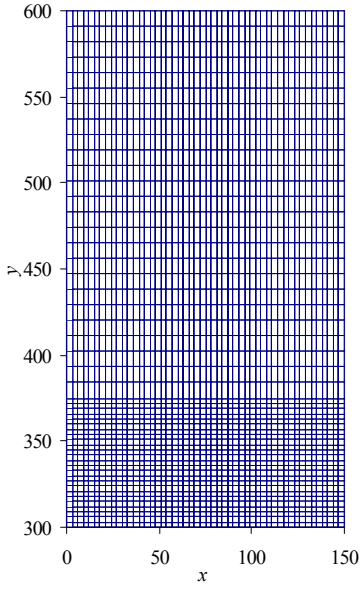

(a)

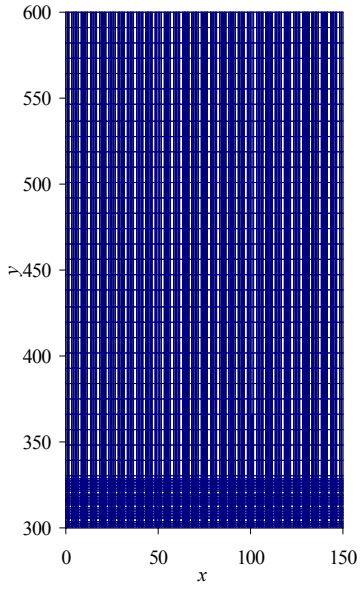

(b)

Figure 13. Coarse (a) and fine (b) mesh for the left half of the specimen.

In the simulation, the first increment of the cohesive crack is 4.4mm, then the cohesive crack propagates by a segment of length 3mm after each step in the coarser mesh, and by three segments of length 1mm each in the finer mesh.

The stresses at the tip of the cohesive crack recovered by SAR are used to judge whether or not the tip will propagate.

The stresses for the finer mesh recovered by AVG and SAR are identical along the circle r = 3.5mm and the line of extension of the crack. Therefore, all stress results presented below are for the coarser mesh, unless otherwise mentioned.

The dimensions of the displacement and length parameters are in mm, and those of the stresses in MPa.

The variation of the tensile stress σ_y and displacement v in y-direction at the central point of the loading edge is shown in Fig. 14. Obviously, it shows no mesh dependency. The evolution of the size of the cohesive zone corresponding to the two branches of the bilinear softening law (5) is shown in Fig. 15. It also reveals very weak mesh dependence. The opening profile and distribution of cohesive stresses in the cohesive zone are shown in Fig. 16, and show some weak mesh dependence. Non-vanishing displacements and stresses along the circle r = 3.5mm, and the line of extension of the crack at loading stages A are plotted in Figs 17 and 18. The displacements on r = 3.5mm from the coarser mesh agree quite well with the finer mesh. The stresses for the coarser mesh obtained by SAR are more accurate than the direct differentiation and AVG, and agree quite well with the finer mesh. Along the line of extension of the crack, the displacement u in x-direction is very sensitive to the mesh size, however the remaining non-vanishing displacement and stress components are not. The agreement between AVG, SAR and the finer mesh is generally very good, however, SAR is better than AVG close to the cohesive crack tip.

Note that close to the cohesive crack tip, the maximum values of the main stresses σ_x and σ_y occur on the cohesive crack face. This feature of the stress distribution has also been noticed by Planas et al. (2003).

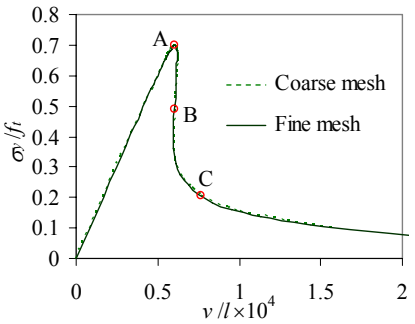

Figure 14. The non-dimensional tensile stress-central extension curves of the uniaxial single-edge notched tension plate.

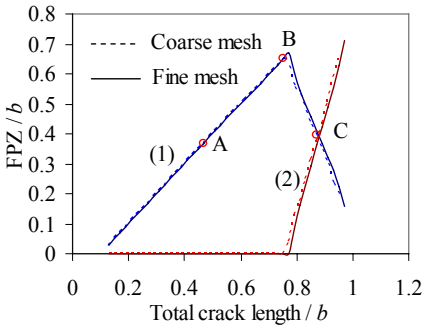

Figure 15. Evolution of the cohesive zone size as the cohesive tip travels through the plate. (1) and (2) correspond to the first and second branches of the bilinear softening diagram (Fig. 3).

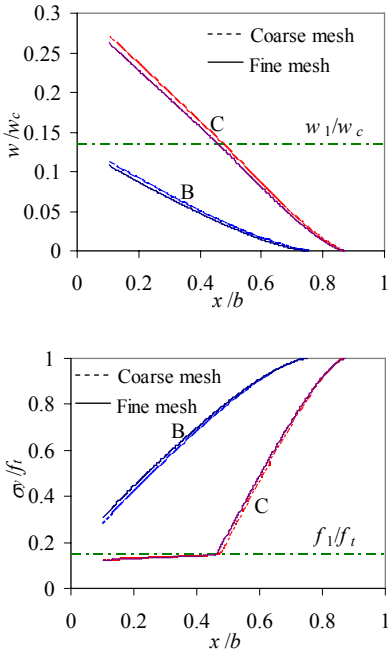

Figure 16. Opening profile and distribution of cohesive stresses in the FPZ at typical loading stages (Fig. 14).

The use of the enrichment function in the XFEM has been noticed to deteriorate the condition of the discrete system (Strouboulis et al. 2001). This does not affect global responses or the stresses and the strain energy. However, it may affect significantly the displacements adjacent to the tip of the cohesive crack, so that a direct comparison of the coarse and fine mesh patterns (Fig. 13) adopted in the analysis is not possible. Hence, we compare instead the displacements relative to the tip of the cohesive crack.

7 DISCUSSION AND CONCLUSIONS

The complete asymptotic expansions for frictionless and frictional cohesive cracks are analogous to the Williams expansions in brittle solids. They are valid for many commonly used separation laws, e.g. rectangular, linear, bilinear, exponential, etc with or without Coulomb friction on crack faces.

Global responses like load – deformation curves, and evolution of the cohesive zone, are not sensitive to the size of the adopted mesh in the XFEM. Local properties like the opening profile and distribution of the cohesive stresses in the cohesive zone, especially crack tip displacements and stresses are more sensitive to the mesh size.

Although no singularity exists at the tip of a cohesive crack, the stresses obtained by direct differentiation of the displacements are not accurate, and cannot be used to predict accurately the growth of the tip. The SAR, which satisfies exactly the non-homogeneous cohesive tractions, gives more accurate results than the widely used AVG adjacent to the crack tip. If high accuracy of the local fields is required (e.g. these fields are use to judge the growth

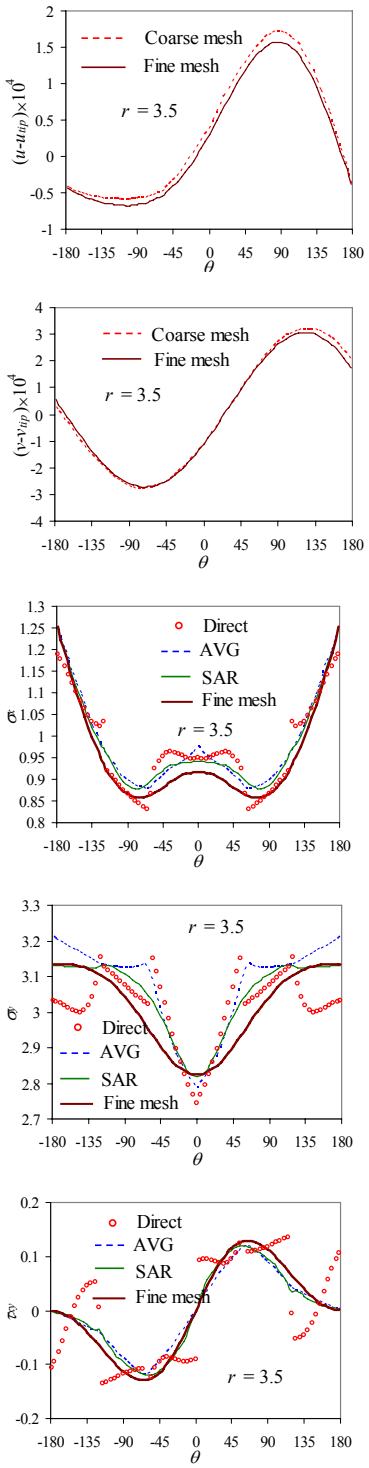

Figure 17. Non-vanishing displacements and stresses along the circle $r = 3.5$mm at loading stage A (Fig. 14).

of the tip), a relatively fine mesh needs to be used together with accurate stress recovery methods, such as SAR.

For mode I cohesive cracks, the stresses recovered by SAR are highly accurate along the line of extension of the cohesive crack, and can be used directly to predict the growth of the crack. For general mixed-mode cracks, further studies are required on whether the SAR stresses at the tip, or on a small circle enclosing a few (e.g. one or two) layers elements around the tip should be used to predict the growth of the crack.

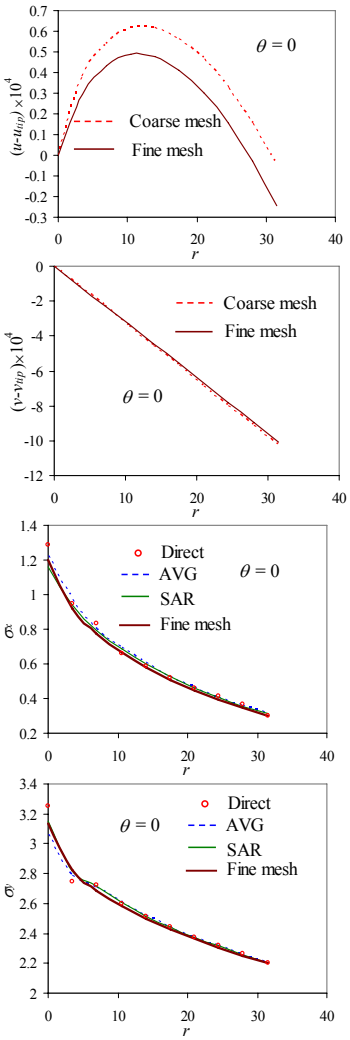

Figure 18. Non-vanishing displacements and stresses along the line of extension of the crack at loading stage A (Fig. 14).

ACKNOWLEDGEMENTS

Financial support from the European Commission KMM-Network of Excellence is gratefully acknowledged.

REFERENCES

Abdalla, H.M. & Karihaloo, B.L. 2004. A method for constructing the bilinear tension softening diagram of concrete corresponding to its true fracture energy. *Magazine Concr Res* 56: 597-604.

Alfaiate, J., Simone, A. & Sluys, L.J. 2003. Non-homogeneous displacement jumps in strong embedded discontinuities. *Int J Solids Struct* 40: 5799-5817.

Cornelissen, H.A.W., Hordijk, D.A. & Reinhardt, H.W. 1986. Experimental determination of crack softening characteristics of normal and lightweight concrete. *Heron* 31: 45-56.

de Borst, R., Gutierrez, M.A., Wells, G.N., Remmers, J.J.C. & Askes, H. 2004. Cohesive-zone models, higher-order continuum theories and reliability methods for computational failure analysis. *Int J Numer Meth Engrg* 60: 289-315.

Elices, M., Guinea, G.V., Gómez, J. & Planas, J. 2002. The cohesive zone model: advantages, limitations and challenges. *Engrg Fract Mech* 69: 137-163.

Hansbo, A. & Hansbo, P. 2004. A finite element method for the simulation of strong and weak discontinuities in solid mechanics. *Comput Meth Appl Mech Engrg* 193: 3523-3540.

Hillerborg, A., Modeer, E. & Petersson, P.E. 1976. Analysis of crack formation and crack growth in concrete by means of fracture mechanics and finite elements. *Cement Concr Res* 6: 773-781.

Karihaloo, B.L. 1995. *Fracture Mechanics and Structural Concrete*. UK: Addison Wesley Longman.

Karihaloo, B.L. & Xiao, Q.Z. 2003a. Linear and nonlinear fracture mechanics. In I. Milne, R.O. Ritchie & B.L. Karihaloo (eds), *Comprehensive Structural Integrity* 2: B.L. Karihaloo & W.G. Knauss (eds), *Fundamental Theories and Mechanisms of Failure* 2.03: 81-212. UK: Elsevier Pergamon.

Karihaloo, B.L. & Xiao, Q.Z. 2003b. Modelling of stationary and growing cracks in FE framework without remeshing: a state-of-the-art review. *Comput Struct* 81: 119-129.

Mariani, S. & Perego, U. 2003. Extended finite element method for quasi-brittle fracture. *Int J Numer Meth Engrg* 58: 103-126.

Moës, N. & Belytschko, T. 2002. Extended finite element method for cohesive crack growth. *Engrg Fract Mech* 69: 813-833.

Moës, N., Dolbow, J. & Belytschko, T. 1999. A finite element method for crack growth without remeshing. *Int J Numer Meth Engrg* 46: 131-150.

Muskhelishvili, N.I. 1953. *Some Basic Problems of Mathematical Theory of Elasticity*. Holland: Noordhoff.

Planas, J., Elices, M., Guinea, G.V., Gómez, F.J., Cendón, D.A. & Arbilla, I. 2003. Generalizations and specializations of cohesive crack models. *Engrg Fract Mech* 70: 1759-1776.

Rubinstein, A.A. 2003. Computational aspects of crack path development simulation in materials with nonlinear process zone. *Int J Fract* 119: L15-L20.

Sih, G.C. & Liebowitz, H. 1968. Mathematical theories of brittle fracture. In H. Liebowitz (ed), *Fracture: An Advanced Treatise* II: 67-190. New York: Academic Press.

Strouboulis, T., Copps, K. & Babuska, I. 2001. The generalized finite element method. *Comput Meth Appl Mech Engrg* 190: 4081-4193.

Wecharatana, M. 1990. Brittleness index of cementitious composite. In B.A. Suprenant (ed), *Serviceability and Durability of Construction Materials*. New York: ASCE Publications.

Wells, G.N. & Sluys, L.J. 2001. A new method for modelling cohesive cracks using finite elements. *Int J Numer Meth Engrg* 50: 2667-2682.

Xiao, Q.Z. & Karihaloo, B.L. 2004. Statically admissible stress recovery using the moving least squares technique. In B.H.V. Topping & C.A. Mota Soares (eds), *Progress in Computational Structures Technology*: 111-138. Stirling, Scotland: Saxe-Coburg Publications.

Xiao, Q.Z. & Karihaloo, B.L. 2005. Recent developments of the extended/generalized FEM and a comparison with the FEM. In X.P. Wu (ed), *Developments and Applications of Solid Mechanics* (Proc of the Symp on Prof M.G. Huang's 90th Birthday): 303-324. Hefei: Press of Univ of Sci and Tech of China.

Xiao, Q.Z. & Karihaloo, B.L. 2006a. Improving the accuracy of XFEM crack tip fields using higher order quadrature and statically admissible stress recovery. *Int J Numer Meth Engrg* 66: 1378-1410.

Xiao, Q.Z. & Karihaloo, B.L. 2006b. Asymptotic fields at frictionless and frictional cohesive crack tips in quasi-brittle materials. *J Mech Mater Struct* 1: 881-910.

Xiao, Q.Z., Karihaloo, B.L. & Liu, X.Y. 2007. Incremental–secant modulus iteration scheme and stress recovery for simulating cracking process in quasi-brittle materials using XFEM. *Int J Numer Meth Engng* (in press).

Zi, G. & Belytschko, T. 2003. New crack-tip elements for XFEM and applications to cohesive cracks. *Int J Numer Meth Engrg* 57: 2221-2240.